FISEVIER

Contents lists available at ScienceDirect

Computer Physics Communications

journal homepage: www.elsevier.com/locate/cpc



Computer Programs in Physics

QuDPy: A Python-based tool for computing ultrafast non-linear optical responses *,**



S.A. Shah ^{a,b}, Hao Li ^a, Eric R. Bittner ^{a,b,*}, Carlos Silva ^{d,c,e}, Andrei Piryatinski ^b

- ^a Departments of Chemistry and Physics, University of Houston, Houston, TX 77204, United States
- b Center for Nonlinear Studies (CNLS), Theoretical Division, Los Alamos National Laboratory, Los Alamos, NM 87545, United States
- ^c School of Chemistry and Biochemistry, Georgia Institute of Technology, Atlanta, GA 30332, United States
- ^d School of Physics, Georgia Institute of Technology, Atlanta, GA 30332, United States
- ^e School of Materials Science and Engineering, Georgia Institute of Technology, Atlanta, GA 30332, United States

ARTICLE INFO

Article history: Received 28 October 2022 Received in revised form 24 July 2023 Accepted 7 August 2023 Available online 18 August 2023

Keywords: Quantum dynamics Nonlinear responses Ultra-fast coherent spectroscopy

ABSTRACT

Nonlinear Optical Spectroscopy is a well-developed field with theoretical and experimental advances that have benefited multiple disciplines, including chemistry, biology, and physics. However, for the accurate interpretation of the corresponding multi-dimensional spectra, there is a need for precise quantum dynamical simulations based on model Hamiltonians. In this article, we present the initial release of our code, QuDPy (Quantum Dynamics in Python), which provides a robust numerical platform for performing quantum dynamics simulations based on model systems, including open quantum systems. A distinguishing feature of our approach is the ability to specify various high-order optical response pathways in the form of double-sided Feynman diagrams through a straightforward input syntax. This syntax outlines the time-ordering of ket-sided or bra-sided optical interactions acting on the time-evolving density matrix of the system. We utilize the quantum dynamics capabilities of QuTip to simulate the spectral response of complex systems, allowing us to compute virtually any *n*-th order optical response of the model system. To illustrate the utility of our approach, we provide a series of example calculations.

Program summary

Program Title: QuDPy

CPC Library link to program files: https://doi.org/10.17632/5xm9pm24cz.1

Developer's repository link: https://github.com/sa-shah/QuDPy

Licensing provisions: MIT License Programming language: Python (v3.7)

Supplementary material: Available as Google Colab Files.

Example 1: https://tinyurl.com/y3j5jmmr Example 2: https://tinyurl.com/37vwntn5

External packages:

- QuTip (v.4.7) and dependencies i.e. Numpy, Matplotlib (https://qutip.org/)
- UFSS Automatic Diagram Generator (https://github.com/peterarose/ufss)

Nature of problem: Accurate quantum simulations of complex systems are required in order to understand and interpret multi-dimensional ultrafast spectroscopic signals. This code provides an open-source/multi-platform method that facilitates the generation of higher-order non-linear optical responses for an arbitrary molecular or material system given a model input Hamiltonian and bath model.

Solution method: We use the double-sided Feynman diagram method [1, 2] to generate (symbolically) a set of response functions corresponding to the n^{th} order non-linear response of the system to a series of laser pulses using the UFSS package [3] We then perform a series of accurate quantum

The review of this paper was arranged by Prof. Blum Volker.

^{★★} This paper and its associated computer program are available via the Computer Physics Communications homepage on ScienceDirect (http://www.sciencedirect.com/science/journal/00104655).

^{*} Corresponding author at: Departments of Chemistry and Physics, University of Houston, Houston, TX 77204, United States. E-mail address: bittner@uh.edu (E.R. Bittner).

dynamics calculations using the QuTip package [4] to generate the numerical response and spectra which correspond to specific experimental conditions.

References

- [1] S. Mukamel, Principles of Nonlinear Optics and Spectroscopy, Oxford University Press, 1995.
- [2] P. Hamm, M. Zanni, Concepts and Methods of 2D Infrared Spectroscopy, Cambridge University Press, 2011.
- [3] Peter A. Rose, Jacob J. Krich, J. Chem. Phys. 154 (2021) 034109.
- [4] J. Johansson, P. Nation, F. Nori, Comput. Phys. Commun. 184 (4) (2013) 1234-1240.

© 2023 Elsevier B.V. All rights reserved.

1. Introduction

Nonlinear, ultrafast spectroscopy has emerged as a powerful experimental tool for probing coherent, light-induced processes in the condensed phase [1–6]. This technique prepares a sequence of ultra-narrow (in time) optical pulses with specific phase-matching conditions that induce a macroscopic polarization response. This polarization is directly linked to the time evolution of the sample under investigation. By varying the time intervals between phasematched pulses, a multi-dimensional map correlating absorption at one time with emission at a later time can be developed. Comparing the experimental signals against robust theoretical models offers tremendous insight into the inner quantum dynamics of a complex system.

The field is mature, with two textbook-level works generally considered introductions [7,8]. However, setting up and performing accurate quantum simulations of complex systems and interacting with the thermal environment has largely been the domain of theoretical groups. Consequently, the community lacks a universal, portable code for conducting such simulations. We present our implementation of a general platform for computing the ultrafast optical response for a generalized system that can be described as a model Hamiltonian in contact with a dissipative environment. Our platform can simulate various molecular and condensed matter systems with finite-dimensional model Hamiltonians. These Hamiltonians can represent physical and chemical systems where the Hilbert space of interest is finite-dimensional, and all other degrees of freedom constitute a bath for this subsystem. Examples include quasi-particles in condensed matter and chemical systems such as phonons, excitons, polaritons, polarons, etc. The platform offers simulation capabilities across a broad spectral range (from NMR to UV-Vis), encompassing various electronic, vibrational, and rotational transitions. Our code, written in Python 3, leverages the open-source QuTip quantum simulation package [9]. It provides users a straightforward way to automatically generate and compute non-linear responses, as specified by a double-sided Feynman diagram given as input. The double-sided diagrams are created using the Automatic Feynman Diagram Generator within the UFSS package, tailored to the desired phase-matching or phase-cycling condition [10,11].

Our code simulates the non-linear optical responses in the impulsive regime, which applies to many ultra-fast optics experiments in which pulse overlap is low or non-existent and the sample dynamics under study are slow compared to the pulse duration [12–14]. These settings are experimentally advantageous as the additional light-matter interaction due to pulse overlap can occlude the signal of interest. Such scenarios require pulse delays that are larger than the temporal width of the pulses used [7,8,12–14].

A typical nonlinear experiment in the visible spectral range uses femtosecond pulses that cover a wavelength range of several nanometers in the spectral domain. Under these conditions, the experiment can be theoretically modeled with infinitely narrow (δ -function) pulses. An additional approximation in this approach is

the dipolar treatment of light-matter interaction; although limiting, it is a staple in multiple nonlinear spectroscopies.

Aside from various home-grown codes localized to various research groups, there are a few codes that are available to the community. The **Spectron/iSpectron** code developed by Mukamel's group provides spectral calculations via two methods. First, through the average amplitudes of Liouville pathways and cumulant expansion of Gaussian fluctuations in reference eigen-energies; second, with molecular configuration-specific Green's function expressions [15]. On the other hand, the Ultrafast Spectroscopy Suite (UFSS) by Rose and Krich obtains nonlinear spectroscopic signatures (for both closed and open quantum systems with finite-dimensional Hilbert space) via perturbative expansion of the wavefunction, and conversion of light-matter interaction with subsequent evolution into a convolution problem with appropriately designed operators. Their method takes into account the temporal profiles of the laser pulses. This results in reduced computational cost for simulation, especially in the case of temporal overlap between different laser pulses. Additionally, the suite provides automatic generation of double-sided Feynman diagrams that has been utilized in this work [10,11]. Briefly, our approach differentiates itself from these packages by computing the direct evolution of the density matrix for the system with intermittent projection with light-matter interaction defining and guiding specific Liouville-space pathways.

We begin with a general overview of the theory of multidimensional spectroscopy, its implementation in our code, and describe its installation and required components. We then present a few model calculations showing how one can set up, compute, and interpret the results. We intend that the code provides a robust and adaptable platform for both theory and experimental groups working in this area. To maintain the article's brevity, the complete code for these simulations is available in Examples 1 and 2 on the Google Colab platform, and the input parameters for various functions and methods in the package are thoroughly explained in the Appendix.

2. Theoretical background and description of the algorithm

In any spectroscopic experiment, one ultimately is measuring a macroscopic polarization of the sample as induced by an incident applied electric field and one can express the polarization in terms of powers of the electric field \vec{E}

$$\vec{P} = \epsilon_o \left(\chi^{(1)} \cdot \vec{E} + \chi^{(2)} \cdot \vec{E} \cdot \vec{E} + \chi^{(3)} \cdot \vec{E} \cdot \vec{E} \cdot \vec{E} + \cdots \right) \tag{1}$$

where $\chi^{(n)}$ are susceptibilities. Since the electric field is a vector, the various susceptibilities are tensors that encode both the amplitude and the electric field polarization of the nonlinear response. However, our current implementation discards the electric field polarization dependence of the non-linear response, focusing only on the overall amplitude of each non-linear term as represented by the dipolar light-matter interaction (discussed below). Such assumptions can be related to polarization-insensitive experiments,

where the input and output pulses' electric field polarizations are not controlled/monitored. For polarization control/sensitivity experiments, the current implementation is equivalent to an isotropic averaged response over all the input and output electric field polarizations.

In isotropic media with inversion symmetry, the polarization must change sign when the optical electric fields are reversed. Consequently, all the even-order terms vanish and the 3rd order term is the lowest-order non-linearity. Under the dipole approximation in light-matter interaction, the observed polarizability is calculated by taking the expectation value of the quantum dipole operator:

$$P(t) = \text{Tr}(\mu \rho(t)) = \langle \mu \rho(t) \rangle \tag{2}$$

where $\rho(t)$ is the quantum density matrix for the system which has evolved under the influence of the external optical fields. This, too, can be expanded in powers of the electric field as

$$P(t) = \sum_{n=1}^{\infty} P^{(n)}(t)$$
 (3)

Each of the terms in this series can be computed within the context of time-dependent perturbation theory by assuming that the applied field interacts with the system at times $\tau_1 < \tau_2 < \cdots \tau_n$. The resulting expression takes the form of a series of nested time integrals and commutation operations,

$$P^{(n)}(t) = \int_{-\infty}^{t} d\tau_n \int_{-\infty}^{\tau_n} d\tau_{n-1} \cdots \int_{-\infty}^{\tau_2} d\tau_1 E(\tau_n) E(\tau_{n-1}) \cdots E(\tau_1)$$

$$\times S^{(n)}(1, 2 \cdots, n), \tag{4}$$

where $S^{(n)}(1,2\cdots,n)$ is the susceptibility given as a series of interactions with the dipole operator $\hat{\mu}$ interspersed by propagation under the Liouville super-operator representing the system dynamics,

$$S^{(n)}(1, 2 \cdots, n) = \chi^{(n)} = \left(-\frac{i}{\hbar}\right)^n \langle \hat{\mu}(n)e^{i\mathcal{L}t_n}[\hat{\mu}(n-1), \cdots e^{i\mathcal{L}t_2}[\hat{\mu}(2), e^{i\mathcal{L}t_1}[\hat{\mu}(1), \rho(0)]]] \rangle$$
 (5)

Note that we have indexed each interaction with the light field by the order in which it appears in the time sequence,

$$\tau_1 = 0$$

$$t_1 = \tau_2 - \tau_1$$

$$t_2 = \tau_3 - \tau_2$$

$$\vdots$$

$$t_n = t - \tau_n$$

and reflects the specific timing of the experimental laser pulses. This is defined for all positive times t_n . The susceptibility can be written as

$$S^{(n)}(1, 2 \cdots, n) = \left(-\frac{i}{\hbar}\right)^n \sum_{i} R_i^{(n)}$$
 (6)

where each $R_i^{(n)}$ is a pathway obtained by the expansion of the nested commutators. One obtains 2^n terms since the dipole operator can act either on the left-side or right-side of the density matrix. However, each term is paired with its complex conjugate,

giving 2^{n-1} unique terms. Further, for an n^{th} order non-linear response, the electric field itself is composed of n pulses,

$$E(t) = \sum_{i=1}^{n} E_i(t) (e^{-i\omega t + \vec{k} \cdot \vec{r}} + e^{+i\omega t - \vec{k} \cdot \vec{r}}),$$
 (7)

such that the simplest 3rd order expression contains $6 \times 6 \times 6 \times 4 = 864$ possible terms. However, most of these terms either vanish or are equivalent. Within the field of ultrafast spectroscopy, these terms are commonly expressed in a diagrammatic representation whereby propagation in time is represented as a vertical line and interactions via the density matrix are incoming or outgoing arrows [7,8]. The last interaction, which is not within the nested commutators represent an outgoing field. The wavevector and frequency of this field comply with the conservation of momentum and energy from previous interactions, resulting in phase-matching and phase-cycling conditions; such that the final wavevector is the sum of wavevectors from all previous interactions and can distinguish rephasing and non-rephasing pathways. Following the usual conventions in this field, one has a series of rules:

- 1. The two vertical lines represent the time evolution of the ket and bra sides of the density matrix with time running from the bottom to the top.
- 2. Interactions with the light field are represented as arrows entering or leaving the diagram at specified times. Since the last interaction occurs outside the nested commutator, it is different and is always represented as an outgoing (dashed) arrow.
- 3. Each diagram has a sign $(-1)^n$ where n is the number of interactions on the right side of the diagram. Each right-hand side interaction carries a minus from the commutator bracket. The last interaction originates outside the bracket and does not contribute a sign.
- 4. An arrow pointing to the right represents an electric field with $e^{-i\omega t + ikr}$ while one pointing to the left represents an electric field with $e^{+i\omega t ikr}$. The emitted light (last outgoing arrow) has a frequency and wavevector given by the sum of the input frequencies and wavevectors.
- Arrows pointing towards the system correspond to excitations of the system, while those pointing away are de-excitations.
- 6. The final trace operation requires that the system is in a population element after the last interaction. The population element in this context is $|n\rangle\langle n|$ instead of a coherence element of the density matrix, represented by $|n\rangle\langle m|$.
- 7. By convention, we will show only diagrams with the last interaction emitting from the ket (i.e., the left side).

The picture that emerges is that at time $\tau_1=0$, the system interacts (from the left or right) with the impinging laser field, which projects a coherence within the system. For example, for a two-state system starting its ground state with $\rho(-\infty)=|0\rangle\langle 0|$ we would have that $\rho(0^+)=(|1\rangle\langle 0|+|0\rangle\langle 1|)$. Each term now evolves under the Liouvillian for time t_1 such that

$$\rho(t_1) = e^{i\mathcal{L}t_1} \rho(0^+) \tag{8}$$

At time t_1 , one has an interaction followed by a time evolution t_i , until the last projection at time t_n when the final signal is observed. Since the projections can be on the right or on the left side of the density matrix, a given experiment can be thought of as a sum over all left and right side interactions. The diagram rules lead to four distinct 3rd order diagrams for a 2-level system and six for a 3-level system (for rephasing and non-rephasing signals or photon echo and virtual echo spectra). The first four are shown on the left in Fig. 1, whereas the additional two are shown on the right.

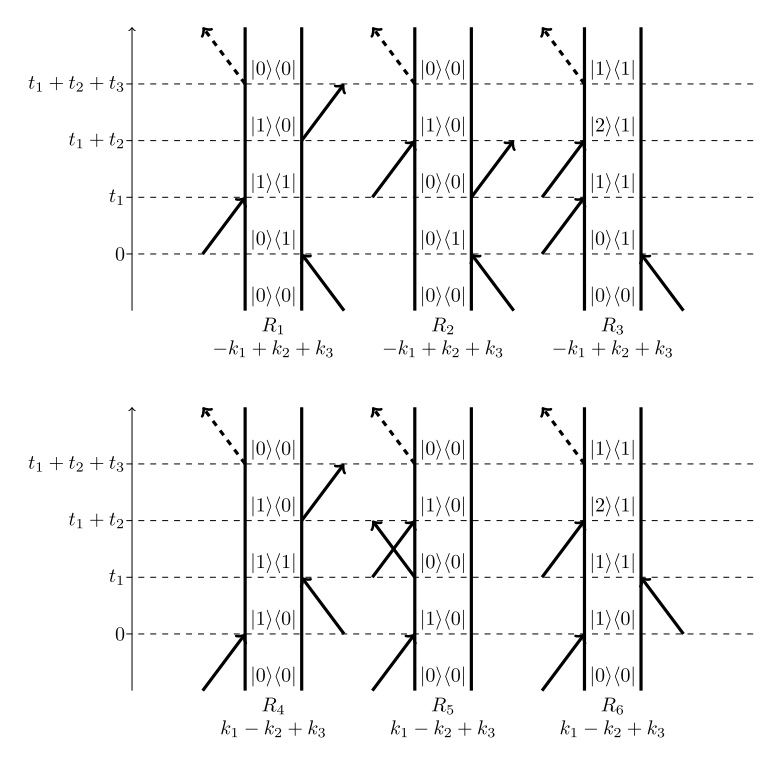


Fig. 1. (Top Row) Rephasing double-sided diagrams for 3rd order response. In a rephasing experiment, the outgoing signal emerges at $k = -k_1 + k_2 + k_3$. (Bottom Row) Non-rephasing double-sided diagrams for 3rd order response. In a non-rephasing experiment, the outgoing signal emerges at $k = +k_1 - k_2 + k_3$. The numbering and notation of these diagrams follow the convention in Ref. [8].

Table 1Summary of response types, operations, and syntax for a 3rd order coherent process corresponding to the diagrams shown in Fig. 1.

Interaction Diagrams		
Response Type	Action	Input Syntax
$R_1(t_1, t_2, t_3) \\ R_2(t_1, t_2, t_3) \\ R_3(t_1, t_2, t_3) \\ R_4(t_1, t_2, t_3) \\ R_5(t_1, t_2, t_3) \\ R_6(t_1, t_2, t_3)$	[B ⁺ , K ⁺ , B, K] [B ⁺ , B, K ⁺ , K] [B ⁺ , K ⁺ , K ⁺ , K] [K ⁺ , B ⁺ , B, K] [K ⁺ , K, K ⁺ , K] [K ⁺ , B ⁺ , K ⁺ , K]	(('Bu',0),('Ku',1),('Bd',2)) (('Bu',0),('Bd',1),('Ku',2)) (('Bu',0),('Ku',1),('Ku',2)) (('Ku',0),('Bu',1),('Bd',2)) (('Ku',0),('Kd',1),('Ku',2)) (('Ku',0),('Bu',1),('Ku',2))

For computational purposes, any diagram can be compactly represented as a time-ordered list of left or right-side operations such as where K^+ and K denote an excitation and a de-excitation on the left (i.e., on the ket), respectively. Similarly, B^+ and B denote a de-excitation and an excitation on the right (i.e., on the bra), respectively. Following the convention introduced by Automatic Feynman Diagram Generator, in QuDPy, these interactions are encoded by 'Ku' and 'Kd' for K^+ and K; similarly, B^+ and B are represented by 'Bu' and 'Bd', respectively [10,11]. Table 1 summarizes 6 possible response functions for a coherent 3rd order process with their equivalent actions and corresponding QuDPy syntax. Notice that the last interaction is not indicated in QuDPy syntax since it always corresponds to a ket-side de-excitation operation by convention.

Note, although only odd-order terms contribute to the polarization in isotropic media, one can also consider interactions that are even-order with respect to the density matrix by measuring the photoluminescence (PL) rather than the polarization. Here, we assume that the final signal is proportional to the relatively slow, spontaneous emission of light from an excited population state (in contrast to the radiated signals arising from off-diagonal coherence elements $|n\rangle\langle m|$ in odd-order spectroscopies) [16]. In this scenario,

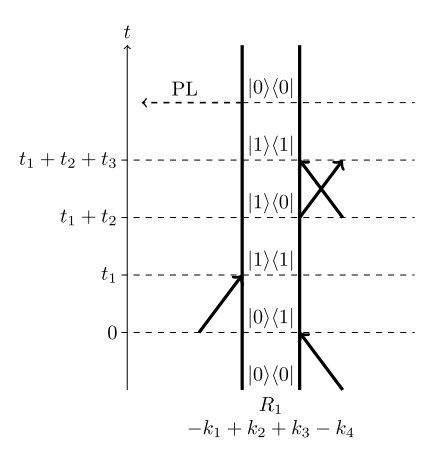


Fig. 2. An example of a 4-th order rephasing diagram for an excited-state emission process specified by ((`Bu', 0), (`Ku', 1), (`Bd', 2), (`Bu', 3)).

one can use a 4-pulse sequence as sketched in Fig. 2, in which the out-going PL reflects the excited state population *vis*.

$$PL_n^{(r)}(t) \propto \langle n|\rho^{(r)}(t)|n\rangle \tag{9}$$

where $\rho^{(r)}(t)$ is the r^{th} order term in the perturbation expansion of the density matrix. This is one of a number of possible interaction pathways and can be input as

$$R_1(0, 1, 2, 3; t) = (('Bu', 0), ('Ku', 1), ('Bd', 2), ('Bu', 3))$$
 (10)

along with 4 times, $\{t_1, t_2, t_3, t\}$, in which the t_2 corresponds to the population waiting time. The last time t corresponds to the observed PL. Additionally, in a comparable experiment, these terms can determine the photo-current generation, with the observed photocurrent being proportional to the population of the final excited state [17–20].

Finally, once response elements (R's) are obtained, the susceptibility can be computed by summation of constitutive responses. Typically, one works in a state space in which the system Hamiltonian is purely diagonal and the interaction with the external laser field is treated as strictly non-diagonal perturbation. As an example, if we take the "system" to be a harmonic oscillator with $H_0 = \hbar \omega (a^\dagger a + 1/2)$ and the light-matter interaction to be mediated by the dipole operator: $\hat{\mu} = \mu (a + a^\dagger)$, one can immediately write down the various response functions in Table 1. For example,

$$R_1(t_1, t_2, t_3) = (-1)^2 \mu^4 \langle a(t_3) a^{\dagger}(t_1) \rho(-\infty) a(t_0) a^{\dagger}(t_2) \rangle \tag{11}$$

in which a(t) is the harmonic oscillator destruction operator in the interaction representation, i.e. $a(t)=e^{i\omega t}a$. However, a generalized physical system is never this simple since the dipole operator can create transitions between multiple quantum states. Moreover, interaction with the environment can induce loss of phase coherence and non-radiative relaxation processes that need to be accounted for in a generalized computational package.

With this in mind, our implementation uses the QuTiP 4.x package to handle all of the setup and propagation of the system variables [9]. Our approach assumes that one can write down the system Hamiltonian and external coupling in terms of a standard set of quantum operators, such as the spin-matrices or harmonic oscillator operators. This includes systems with time-dependent Hamiltonians, systems interacting with complex bath degrees of freedom, cavity QED, polaritons, and a wide variety of open-quantum systems. The current version of QuTip includes both Lindblad and Redfield equation integrators which are continuously improved upon to optimize both numerical efficiency and memory overhead. We present some of the main details on the methods and capabilities for defining system Hamiltonians and system-bath interactions in the appendix and refer the interested reader to the thoroughly detailed documentation of the QuTip package [21].

Our implementation interrupts the QuTip mesolve() routine at the specified intervals performs the required projection, and then allows the propagation to continue. Rather than propagating the operators in the interaction representation, we propagate the density matrix in the Schrödinger representation and then act with the perturbation at specified times.

For example, to simulate the R_1 rephasing diagram, we first define a quantum system Hamiltonian, H, and transform all system operators into a basis in which H is diagonal,

$$\tilde{H} = e^{-S}He^{+S}$$

We then write the dipole operator (and all other operators for that matter) in the eigenbasis as

$$\tilde{\mu} = e^{-S} \mu e^{+S} = \tilde{\mu}_+ + \tilde{\mu}_-,$$

where $\tilde{\mu}_+(\tilde{\mu}_-)$ is the part of the transformed dipole operator that leads to a ket's excitation (de-excitation) and vice-versa for a bra. This can be done analytically or numerically within QuTip. Similarly, we define the initial density matrix, $\rho(-\infty)$, in the eigenbasis of \tilde{H} . All the operators must be defined as quantum operators within the same Fock space. QuTip will return an error if all quantum operators are not defined within the same Fock or Hilbert space.

QuTip provides an efficient implementation for including system/bath interaction using either Redfield theory [22] or Lindblad theory [23]. Under the Lindblad approach, the density matrix evolves according to

$$\frac{d}{dt}\rho = -\frac{i}{\hbar}[H_{sys}, \rho] + \sum_{i} \gamma_{i}(L_{i}\rho L_{i}^{\dagger} - \frac{1}{2}\left\{L_{i}^{\dagger}L_{i}, \rho\right\})$$
 (12)

where $\{L_i\}$ is a set of orthonormal operators defined in the operator space of the system Hilbert space, and γ_i are real, positive rates associated with the bath fluctuations and dissipation. The curly brackets $\{\cdot,\cdot\}$ denote the anticommutator.

At t=0, we apply the first projection and proceed to generate a specific Liouville-space trajectory by alternatively propagating and projecting. For example, the R_1 diagram is specified with the OuDPy syntax as

We assume that the initial density matrix is stationary up until time t=0, at which we apply the first interaction. In this case, it is a bra-side (right-side) excitation, corresponding to

$$\rho((Bu); 0^+) = (\rho(-\infty)\tilde{\mu}_-).$$

This is not the full density matrix, simply one time-evolved contribution following a sequence of steps through the Liouville space. The full-density matrix is a sum of all possible projections and propagations. Secondly, the interactions are local in time since we assume each pulse to be essentially a δ -function in time. This term is propagated under the system/bath Liouvillian operator, \mathcal{L} , to time t_1 ,

$$\rho((Bu); t_1) = e^{i\mathcal{L}t_1}\rho((Bu); 0^+) = e^{i\mathcal{L}t_1}(\rho(-\infty)\tilde{\mu}_-),$$

at which time we act again, in this case on the ket-side excitation with $\tilde{\mu}_+$:

$$\rho((Bu, Ku); t_1^+) = \tilde{\mu}_+ \rho((Bu); t_1) = \tilde{\mu}_+ \left(e^{i\mathcal{L}t_1} (\rho(-\infty)\tilde{\mu}_-) \right).$$

Again, this is propagated to time $t_1 + t_2$ at which time we act on the bra-side with a de-excitation:

$$\rho((Bu, Ku, Bd); (t_1 + t_2)^+)$$

$$= \left(e^{i\mathcal{L}t_2} \left(\tilde{\mu}_+ e^{i\mathcal{L}t_1} \left(\rho(-\infty)\tilde{\mu}_-\right)\right)\right) \tilde{\mu}_+. \tag{13}$$

Finally, we propagate for the third time interval and act (on the ket-side) with the final de-excitation to produce the term contributing to the full polarization signal. For the case at hand, we have

$$R_{1}(t_{1}, t_{2}, t_{3}) = \left\langle \tilde{\mu}_{-} e^{i\mathcal{L}t_{3}} \left(\left(e^{i\mathcal{L}t_{2}} \left(\tilde{\mu}_{+} e^{i\mathcal{L}t_{1}} \left(\rho(-\infty) \tilde{\mu}_{-} \right) \right) \right) \tilde{\mu}_{+} \right) \right\rangle. \tag{14}$$

Similar expressions can be written for the other five response diagrams. Note, that if $\mathcal L$ carries an explicit time dependency, then each propagation step needs to be taken as a time-ordered operation

Continuing with the example of 3rd order response, in a typical experiment, one scans the t_1 and t_3 intervals for a fixed t_2 interval. Since during t_2 , the system is in a population state of the density matrix, t_2 is referred to as the "population time". One then performs a 2D Fourier transform with respect to t_1 and t_3 for a fixed population time. Generally speaking, the signal along the diagonal provides a correlation between the absorption and emission spectra of the system for a given population time, and the off-diagonal features correspond to the coherences between the states. Note that the off-diagonal coherence signal may connect both bright and dark (non-emissive) states. Fig. 3 gives a general overview of the information that can be obtained via a 3rd order polarization measurement. In Fig. 3(a), the symmetric offdiagonal features indicate that the two states (labeled $|a\rangle$ and $|b\rangle$) share a common ground state ($|g\rangle$). In Fig. 3(b) the absence of offdiagonal features indicates that the states are decoupled, whereas

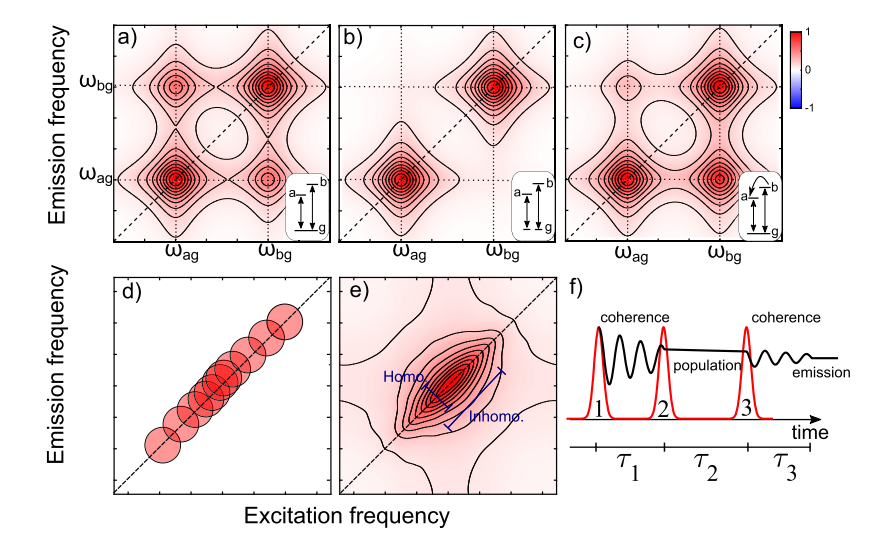
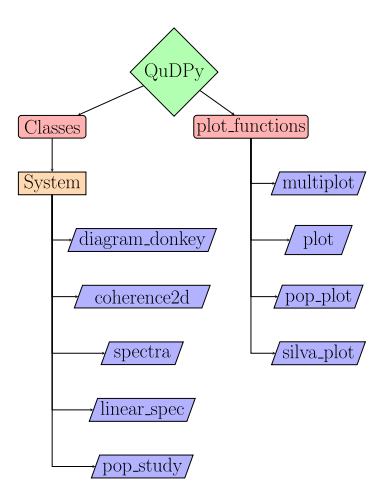


Fig. 3. Example of a 2D spectra of a system with two excited levels $|a\rangle$, $|b\rangle$ and a ground state $|g\rangle$. (a) The intensity spectrum is symmetric along the diagonal since the states share a common ground, (b) the states are decoupled, (c) coupling of the $|b\rangle$ and $|a\rangle$ leads to relaxation of $|b\rangle$ towards $|a\rangle$, which translates to an asymmetric amplitude of the off-diagonal peaks. Insets in (a-c) show the energy diagrams for corresponding mechanisms, and the transition frequencies are labeled by ω 's. (d-e) indicate the modulus of a rephasing 2D spectrum for an inhomogeneous system that consists of a collection of emitters, where, in (d) each resonant frequency is decoupled from the others and is schematically represented by a red circle. The homogeneous width of each emitter, represented by the size of the circle, is measurable along the anti-diagonal. (e) The total signal forms an elongated peak along the diagonal (inhomogeneous broadening). (f) Pulse sequence used to perform a multi-dimensional coherence spectroscopic measurement for obtaining 3rd-order polarization response. (Reprinted from Ref. [24].) (For interpretation of the colors in the figure(s), the reader is referred to the web version of this article.)

in Fig. 3(c) the asymmetry in the off-diagonal features are indicative of dynamical evolution between two excited states. Moreover, the overall structure of the diagonal line shapes indicates the local environment that each state samples. As seen in Fig. 3(d, e), inhomogeneous broadening along the diagonal arises from the statistical sampling of various local environments within the sample; whereas the elongation across the anti-diagonal results from the homogeneous broadening mechanisms. Consequently, this technique separates the homogeneous and inhomogeneous contributions to the overall line shape [2]. Consequently, one obtains a wealth of dynamical information regarding the inner workings of a quantum system through the use of coherent, multi-dimensional spectroscopy.

Our approach allows one to compute the quantum dynamics associated with an arbitrary model Hamiltonian using QuTip (v4) quantum optics package [9]. The QuTip package is robust, easy to use, and has developed a sizable user group spanning multiple areas of atomic and molecular physics. We also incorporate a symbolic approach for determining the irreducible/non-vanishing double-sided Feynman diagrams [10], which provides a straightforward way to compute the 2D responses in the time domain. Additionally, our method leverages the efficient Fast-Fourier Transform (FFT) capabilities in Numpy for efficient conversions to the frequency domain. Lastly, we note that our approach is not limited to 3rd-order non-linear responses. In principle, one can use our approach to simulate arbitrary order experiments with arbitrarily complicated system/bath Hamiltonians, limited only by the computational resources (and time) available to the user.

The disadvantage of our current implementation is that it assumes the interaction with the external laser field is purely impulsive, acting only at a single instant. However, this is not an extreme limitation since the experimental setups we are most interested in studying, achieve this limit using temporally narrow pulses that span the entire spectral frequency range of the system. Additionally, the pulse overlap is often an experimentally undesirable situation that results in coherence spikes and the inclusion of additional diagrams in the signal of interest, a situation most experiments tend to avoid [10,25]. Finally, it is fairly straight-forward



 ${\bf Fig.~4.}$ QuDPy structure, the subroutines are shown in red, and the functions are shown in purple.

to implement finite-sized pulses within our approach, we reserve this for future releases of our method.

3. Downloading and installation

QuDPy relies on only a few packages, namely QuTip for quantum dynamics, UFSS for diagram generation, and supporting packages such as NumPy and Matplotlib. The QuDPy package can be installed with a simple command pip install qudpy==1.x.x where 1.x.x is the version number. The installation process automatically installs any required packages in case they are not installed. The online GitHub repository for the package can be found here (https://github.com/sa-shah/QuDPy).

QuDPy comprises two subroutines i.e., Classes and plot_functions. The program's structure is shown in Fig. 4. The details of methods and functions in the package (along with their input and output parameters) are provided in the Appendix.

4. Example calculations

Before giving two worked examples, we give an overview of the typical workflow for using our approach. This section does not provide the complete code as it is documented in Examples 1 and 2, available on Google Colab (links on the front page).

4.1. Typical workflow

A typical work-flow using our approach begins by defining the system Hamiltonian using the QuTip package and then initializing the diagram-generation code in UFSS using a desired phasematching/phase-cycling condition [10,11]. The diagram-generation step is formally agnostic of the system Hamiltonian at this point and these two initial steps can be easily swapped. Furthermore, the user can provide custom diagrams without invoking UFSS, provided the diagrams are in the format required by the UFSS routine.

The system setup can be accomplished using the System() command provided in the QuDPy package e.g. a custom system with Hamiltonian Hd, light-matter interaction operator A, dipole operator mud, collapse operator list c_ops and density matrix rho, can be created by

```
sys=System(H=Hd,
    a=A,
    u=mud,
    c_ops=[c1d,c2d,c3d,c4d],
    rho=rho)
```

This is provided as a utility routine for setting up the system and its associated quantum Fock space (that depends on the basis used to define Hamiltonian and interaction operator). We next provide two worked examples to illustrate how to use our code for performing spectral simulations.

4.1.1. Inclusion of light-matter interaction in quantum evolution

In addition to the evolution under system bath interaction, the system also observes light-matter interaction in accordance with a given double-sided diagram. The Automatic Diagram Generator in UFSS generates the diagram for phase-matching or phase-cycling conditions. For example, consider the case of $R_{1,2,3}^{(3)}$ in the phase matching direction $-k_1+k_2+k_3$; the corresponding diagrams can be generated by:

```
import ufss
R3rd = ufss.DiagramGenerator()
R3rd.set_phase_discrimination([(0,1),(1,0),(1,0)])
d = np.array([1]) # assigning pulse durations
R3rd.efield_times = [d, d, d, d]
# Setting pulse delays
time_ordered_diagrams_rephasing = R3rd.get_diagrams([0,100,200,200])
[R3, R1, R2] = time_ordered_diagrams_rephasing
rephasing = [R1, R2, R3]
```

In the code above, each pulse is considered 1 fs long with pulse delays t_1, t_2, t_3 of 100, 200, and 200 fs, respectively. (Note: these delays are arbitrary at this point and selected only to ensure non-overlapping pulses.) The double-sided diagrams contain R1, R2, and R3. These diagrams then become inputs for calculating the spectral response with appropriate system evolution.

4.1.2. Imposing time gating for light-matter interactions

Given a system and a double-sided diagram, the density matrix evolves with the appropriate master equation until a light-matter interaction is encountered as dictated by the diagram. The corresponding raising or lower operation is applied from the left or right on the density matrix. Afterward, the density matrix becomes the initial density matrix for the next step of evolution under the same master equation as before till the next light-matter interaction. This pattern is repeated for all light-matter interactions. For

experimentally observable spectroscopic response, only the final state after the last light-matter interaction is important; however, states throughout the evolution can be saved for inspection.

4.1.3. 2D coherence

In a particularly useful experimental scheme, the coherence generated under different light-matter interactions in a double-sided diagram is utilized to probe intra-material interactions spectroscopically. In this approach, two-time delays are tuned, while all others are fixed. The resulting final density matrices generate 2D spectra by computing $\langle \mu \rangle$. Experimental feasibility or the desired spectroscopic frequency precision determines the scan range for adjustable time delays.

For example in R_1 , coherences are generated during time intervals t_1 and t_3 (i.e. $|0\rangle\langle 1|$ and $|1\rangle\langle 0|$). The set of final states in corresponding 2D coherence with a t_1 and t_3 range of 200 fs each and t_2 fixed at 20 fs, can be generated by

```
sys1 = System().
t1, t2, t3 = (200, 20, 200)
statesR1 = sys1.response2D_pop(R1, t1, t2, t3)
```

These can then generate spectra with in-built functions that compute $\langle \mu \rangle$ from these states.

4.2. Fourier transform and resolution in frequency domain

To generate high-resolution 2D coherence spectra, follow these guidelines for efficient utilization of computational resources:

- Increase time-domain resolution for a larger scanned frequency range in the spectra.
- Use the maximum difference between eigenvalues of the system Hamiltonian to estimate the minimum time-step via the Nyquist theorem for a faithful simulation. Note the step size must be small enough to support QuTip differential equation solvers (QuTip will output an appropriate warning otherwise).
- Select a large scan range for the time domain for improved frequency domain resolution.
- If the system loses coherence quickly, avoid additional system evolution, as it would only result in smoothing spectral features. Instead, use smoothing functions while plotting the spectra.
- For inspection of system evolution and expectation values of important observables, utilize the diagram_donkey test run before committing to a full-scale simulation.

4.3. Example 1: excitation exchange coupling between chromophores

In the example which follows, we consider two coupled oscillators with Hamiltonian:

$$H/\hbar = \omega_1 a^{\dagger} a + \omega_2 b^{\dagger} b + I(a^{\dagger} b + b^{\dagger} a) \tag{15}$$

Physically, this corresponds to a system composed of two chromophores that can exchange quanta via the exchange coupling, J, which can be either positive or negative. The transition dipole operator is the sum of the dipole operators for each oscillator,

$$\hat{\mu} = \mu_A(a + a^{\dagger}) + \mu_B(b + b^{\dagger}). \tag{16}$$

In this example, we also assume each oscillator is coupled to a thermal bath which relaxes each to a thermal population. This is a general model for a wide range of systems encountered in chemical physics.

The complete Python code for this model is provided in the Example 1 Jupyter notebooks on Google Colab. Once the system has been set up, we are ready to compute something and it is

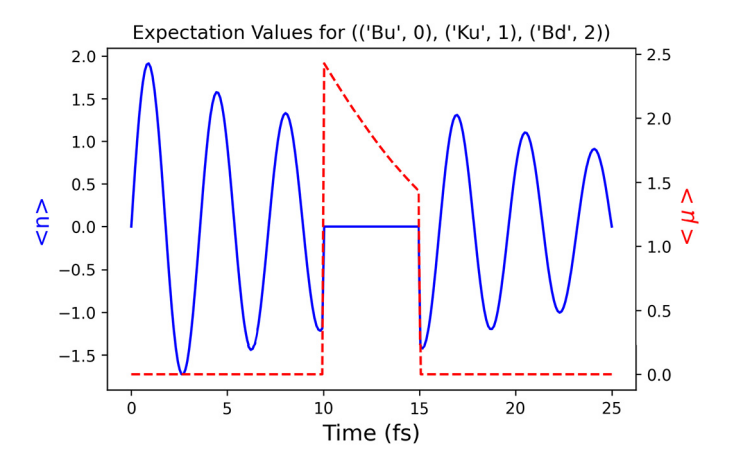


Fig. 5. Results from diagram_donkey show the expectation values of system dipole (red dashed) and excitation number (blue solid) operators for a R_1 diagram with a coherence time of 5 and 10 fs for the first and second coherence, and a population time of 5 fs. The results reveal the population relaxation and loss of coherence from system-bath interactions.

useful to examine the populations and coherences produced by the R_1 diagram.

states = sys.diagram_donkey(
$$[0,5,10,20],[R1],r=10$$
)

The pulse arrival times of 0, 5, 10, 20 fs and a resolution of 10 steps per fs are selected arbitrarily to illustrate the functionality. This produces a plot showing the populations and coherences versus time as shown in Fig. 5. Notice that from time t=0 to 5 fs, the system evolves as a coherence $|0\rangle\langle1|$, from 5 fs to 10 fs, the system is projected onto a population $|1\rangle\langle1|$ where it undergoes non-radiative relaxation. As noted above, this time period is called the *population time*. At 10 fs, it is again projected onto a coherence, this time $|1\rangle\langle0|$ where it evolves for an additional 10 fs before being projected back down to the $|0\rangle\langle0|$ ground state. It is important to note that the coherences and populations are in the eigenbasis and not with regards to the primitive (pre-diagonalized) system.

A full simulation will involve independently scanning t_1 and t_3 for a fixed t_2 population time. This is accomplished using coherence2d() routine as illustrated here.

Here, we are first passing a series of time-delays t_1 , t_2 , and t_3 , a list of diagrams, and the indices of time delays that will be scanned e.g., 0 and 2. Further options include adjusting the temporal resolution for simulation and using parallel computing (if available); however, they are omitted from the current example for clarity. The selection of scan range in this example, although arbitrary, is typical of ultrafast femtosecond experiments, but it can be adjusted to the desired theoretical and practical requirements. This step typically requires the most computational effort since we repeat the time propagation to cover the specified temporal range with a fine-enough grid of points to resolve the spectral features. The calculations return, among other things, a 2D list of dipole operator expectation values for every choice of t_1 and t_3 . This response list is the main ingredient required for calculating the observable spectra. We can now analyze the calculations and compute the 2D spectra using the spectra() function as follows:

spectra_list, extent, f1, f2 = sys.spectra(response_list)

Fig. 6 displays this example's 2D spectra for a given t_2 population time. The Fourier transform routine will return the full frequency range spanning both positive and negative frequencies; however, in the plots, only the fourth and first quadrants are shown for rephasing and nonrephasing signals, respectively. Furthermore, the y-axis is inverted for the rephasing diagrams following the conventions of ultrafast spectroscopy.

4.4. Example 2: cavity QED using QuDPy

In this example, we consider a driven/dissipative open quantum system consisting of a finite number of independent two-state atoms coupled to a quantized mode of the radiation field (Dicke model) [26]. The Dicke model shows a mean-field phase transition to a super-radiant phase when the coupling between light and matter crosses a critical value. The Dicke transition belongs to the Ising universality class and has been used to model several cavity quantum electrodynamics experiments [27–29]. While Dicke superradiant transition is analogous with the lasing instability, lasing and Dicke superradiance belong to different universality classes [30].

In this example, we shall assume that an open-quantum system consisting of a single cavity mode coupled to N independent 2-level systems is in turn probed by an external laser field that acts as a time-dependent perturbation. The Hamiltonian for the model reads

$$H = \hbar \Omega_c a^{\dagger} a + \hbar \sum_{i=1}^{N} \omega_j \sigma_z(j) + \frac{2\lambda}{\sqrt{N}} (a + a^{\dagger}) \sum_i \sigma_x(j)$$
 (17)

where Ω_c is the frequency of the (cavity) mode and $\{\omega_j\}$ are the transition frequencies of the individual spins and λ parameterizes the coupling strength between spins and cavity mode. In our worked model, we take all the spins are to be identical. Under this assumption, we can define the total spin operators

$$S_{\alpha} = \sum_{i} \sigma_{\alpha}(j) \tag{18}$$

which satisfies the spin algebra $[S_x, S_y] = i\hbar S_z$. Using these operators, the Hamiltonian simplifies to

$$H = \hbar \Omega_c a^{\dagger} a + \hbar \omega S_z + \frac{2\lambda}{\sqrt{N}} (a + a^{\dagger}) S_X$$
 (19)

This simplifies the numerical studies by reducing the Hilbert space for the spins from 2^N to 2S + 1 with $S \le N/2$. Lastly, the third term is the coupling between the cavity mode and the two-level systems. The \sqrt{N} is introduced so that the coupling becomes a constant in the limit of $N \to \infty$. As such, we define the coupling

$$g = \frac{2\lambda}{\sqrt{N}} \tag{20}$$

and write the system Hamiltonian as

$$H/\hbar = \Omega_c a^{\dagger} a + \omega S_z + g(a + a^{\dagger}) S_x \tag{21}$$

In these units, the critical coupling occurs at $g_c = \sqrt{\Omega_c \omega}/2$. The Dicke model itself is related to several other models in quantum optics. Specifically, when N=1, it is the Rabi model. If the counter-rotating terms $(a\sigma^-(j)$ and $a^\dagger\sigma^+(j))$ are excluded, the model is termed the Jaynes-Cummings model for N=1 and the Tavis-Cummings model for N>1.

In this example, we consider the driven/dissipative Dicke model in which the density matrix evolves according to the quantum master equation

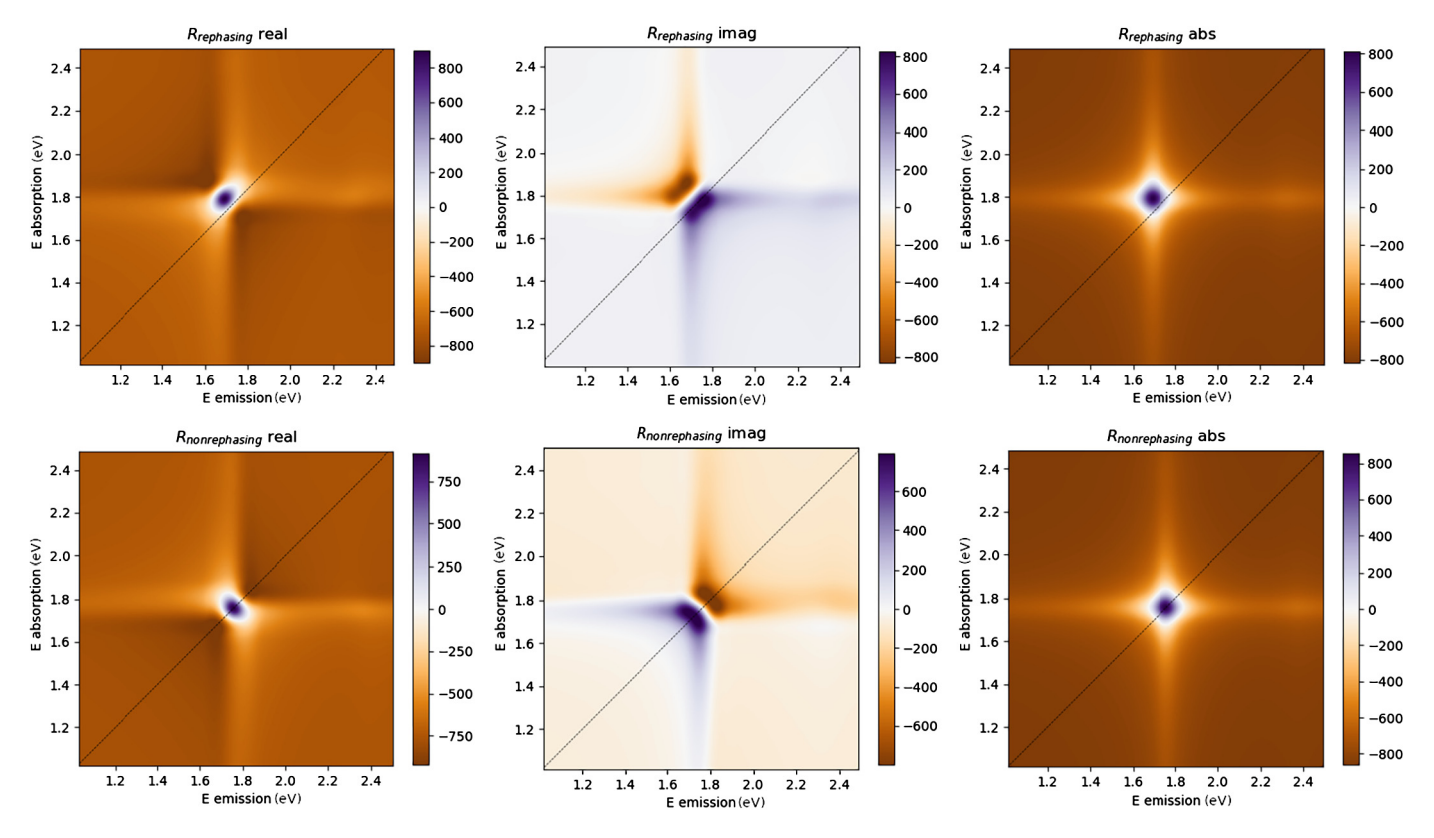


Fig. 6. Frequency domain response (i.e. spectra) for two-time correlation. The top row displays the sum of rephasing diagrams R_1 , R_2 , and R_3 with left, center, and right plots showing real, imaginary, and absolute values, respectively. The bottom row represents the same for the sum of nonrephasing diagrams R_4 , R_5 , and R_6 . These spectra only show the first quadrant for the non-rephasing and the fourth for rephasing (with an additional inversion of y-axis for rephasing).

$$\frac{d}{dt}\rho = \frac{1}{i\hbar}[H,\rho] + \sum_{\alpha} \gamma_{\alpha} \left(L_{\alpha}\rho L_{\alpha}^{\dagger} - \frac{1}{2} \left\{ L_{\alpha}^{\dagger} L_{\alpha}, \rho \right\} \right) \tag{22}$$

in which we include terms for cavity decay and pumping, atomic relaxation, atomic dephasing, and collective decay. Our simulations are initialized by first requiring the system's density matrix to be in a steady state with regards to the unperturbed quantum master equation, i.e., $d\rho_{ss}/dt=0$. Once $\rho_{ss}=\rho(-\infty)$ has been determined, either via numerical relaxation or analytically, the simulation proceeds as above. For this, we assume a thermal population of photons in the cavity mode (as determined by the pumping intensity) and define Lindblad operators

$$L_1 = \sqrt{\kappa (n_{th} + 1)a} \tag{23}$$

$$L_2 = \sqrt{\kappa n_{th}} a^{\dagger} \tag{24}$$

where κ is the photon exchange rate between the cavity mode and the external bath.

Within our model, we assume that the driven/dissipative cavity+spins system is additionally probed by a series of perturbative ultrafast pulses that exchange quanta with the cavity mode via

$$H_{cav/laser} \propto \mu_{cav}(b_{laser}^{\dagger} a + a^{\dagger} b_{laser}).$$
 (25)

Taking the applied laser field to be semi-classical, we can write this as

$$H_{cav/laser} \propto \mu_{cav}(E(t)a + E^*(t)a^{\dagger})$$
 (26)

where E(t) is the electric field of the applied probe pulses and μ_{cav} is the transition dipole of the cavity. This assumption is based on the fact that the experimental signals correspond to the macroscopic polarizability of the entire cavity system. Fig. 7 provides a pictorial representation of the proposed experiment.

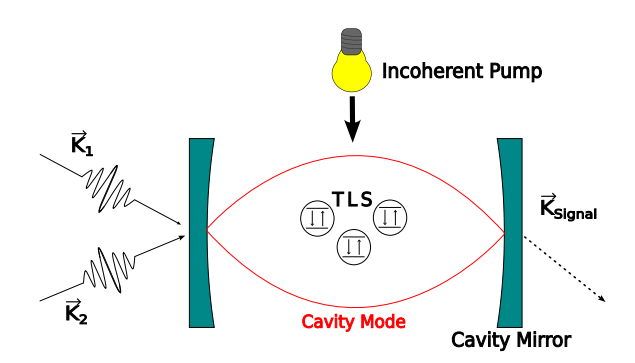


Fig. 7. Third order response for the Dicke Model system. The cavity contains two-level systems (TLS) that interact with each other and the cavity mode (represented by a red curve). The cavity is pumped with an incoherent light source (bulb), and the system is probed with two pulses K_1 and K_2 . The generated signal in a proper phase-matching direction is K_{signal} .

In our examples, we consider the non-linear 3rd order response for a resonant cavity $\hbar\Omega_c=\hbar\omega_j=1$ which has a critical coupling of $\lambda_c=\frac{\sqrt{\Omega_c\omega}}{2}=1/2$. The simulation is performed with a cavity-spin coupling strength of 0.25, N=6 spins, and a 6-state basis for the cavity mode. The cavity pumping/relaxation rate κ is set at 0.05. The spin dephasing is also introduced as $\sqrt{0.15}S_z$. These are chosen as model parameters and are not specific to the particular physical system. The detailed list of parameters and additional information is provided in the relevant Jupyter notebooks in the SI/GitHub repository.

Fig. 8 shows the predicted 2D coherence spectra for our model system. In this case, one can clearly see symmetric off-diagonal coherences between the two diagonal peaks corresponding to the lower and upper polariton (LP and UP) states of this system. In this

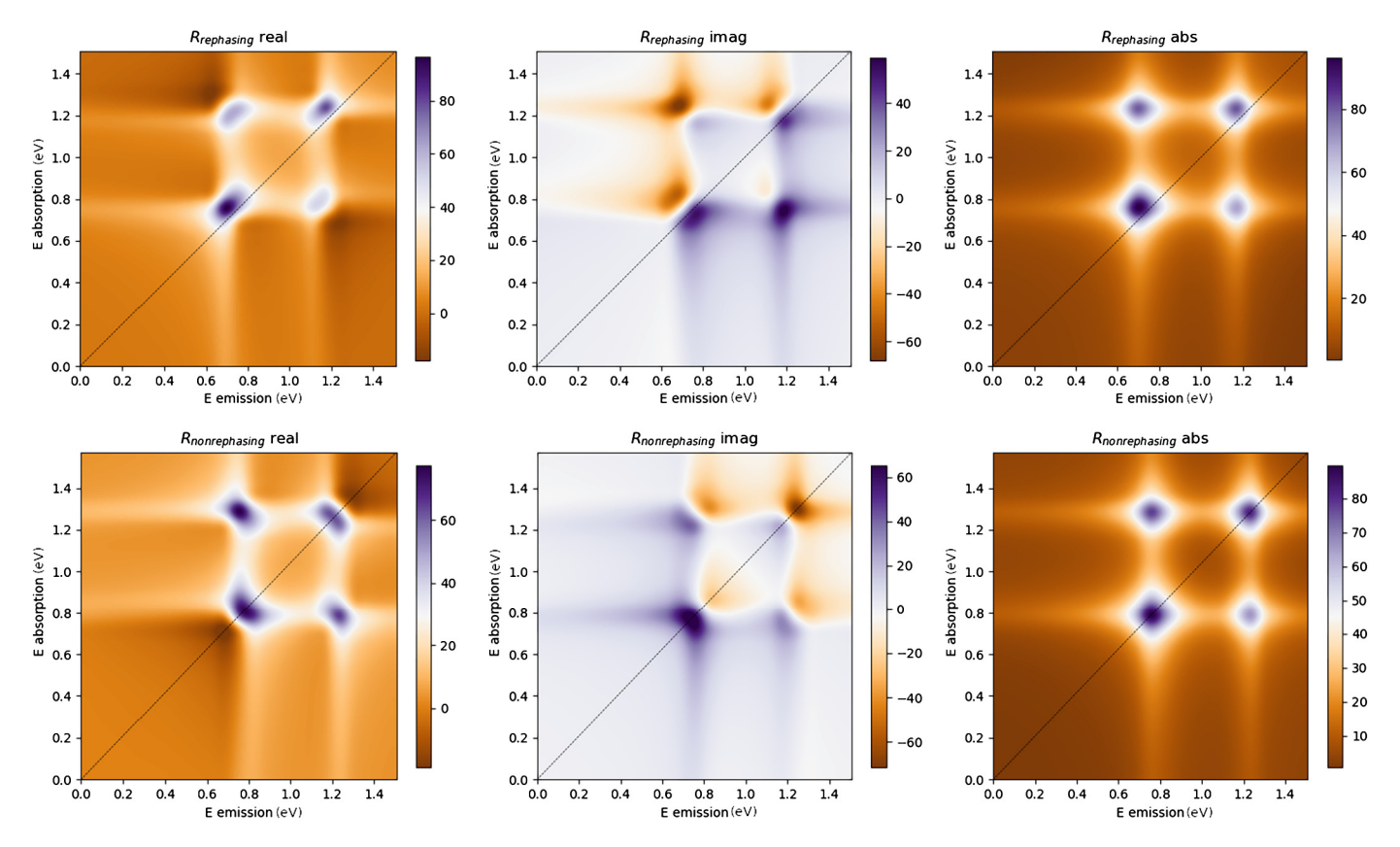


Fig. 8. 2D coherence spectra of response for example 2. The top row displays the sum of rephasing diagrams R_1 , R_2 , and R_3 , and the bottom row represents the same for the sum of nonrephasing diagrams R_4 , R_5 and R_6 . The left, center, and right columns show real, imaginary, and absolute values, respectively. Only the first quadrant for the non-rephasing and the fourth for rephasing diagrams are shown.

case, both LP and UP are connected to a common ground state. Physically, this can be understood since in setting up the problem we transformed the cavity operators a and a^{\dagger} to the eigenbasis of the Dicke Hamiltonian. More complex dynamics can be introduced (for example) by including *incoherent* relaxation pathways via additional Lindblad operators.

5. Discussion

We present here the first-release of our generalized package for simulating non-linear spectral responses observed in modern ultrafast spectroscopy. While our examples have focused upon optical signals, the approach we have adopted can be used to model a wide-range of physical problems with significant ease and control, allowing the end-user to rapidly create model Hamiltonian systems and compute accurate responses. We have avoided a detailed analysis of the results to keep the discussion focused on introducing the package and its use. Future releases of this code will include the facility for more complex pulse-shapes, time-dependent system Hamiltonians, electric field polarization, and the means to connect the approach to ab initio treatments of molecular systems that can provide an explicit Hamiltonian with excitation manifolds and inter-band transition dipoles (as QuTip is capable of simulating the appropriate quantum dynamics provided by the explicit Hamiltonian). We believe that the code will have tremendous utility within the ultrafast spectroscopy user community as well as a useful pedagogic tool for courses on modern spectroscopic methods.

CRediT authorship contribution statement

S.A. Shah: Conceptualization, Formal analysis, Methodology, Visualization, Writing – original draft. **Hao Li:** Formal analysis.

Eric R. Bittner: Conceptualization, Funding acquisition, Methodology, Project administration, Supervision, Writing – review & editing. **Carlos Silva:** Conceptualization, Funding acquisition, Project administration. **Andrei Piryatinski:** Conceptualization, Formal analysis, Funding acquisition.

Declaration of competing interest

The authors declare that they have no known competing financial interests or personal relationships that could have appeared to influence the work reported in this paper.

Data availability

Data will be made available on request.

Acknowledgements

The work at Georgia Tech was funded by the National Science Foundation (DMR-1904293). CS acknowledges support from the School of Chemistry and Biochemistry and the College of Science at Georgia Tech. The work at the University of Houston was funded in part by the National Science Foundation (CHE-2102506, DMR-1903785) and the Robert A. Welch Foundation (E-1337). The work at LANL was supported by the U.S. Department of Energy through the Los Alamos National Laboratory. Los Alamos National Laboratory is operated by Triad National Security, LLC, for the National Nuclear Security Administration of U.S. Department of Energy (Contract No. 89233218CNA000001).

Appendix A. OuTip functions and methods

A.1. States and operators

Different typical states can be defined as follows:

- Fock state ket and density matrix by basis(N, m) and fock_dm(N,p), here m and p are the occupied energy levels and N is the size of Hilbert space.
- Coherent state and density matrix by coherent (N, alpha) and coherent_dm(N, alpha), where alpha is the eigenvalue for requested coherent state.
- For thermal density matrix thermal_dm(N,n) with n as particle number expectation value.

For common operators, following built in options are available.

- Lowering: destroy(N)
- Raising: create(N)
- Number: num(N)
- Single mode displacement: displace (N,alpha), where alpha is the displacement amplitude.
- Single mode squeeze: squeeze(N,sp) with sp as the squeezing parameter.
- Sigma X: sigmax()
- Sigma Y: sigmay()
- Sigma Z: sigmaz()
- Sigma plus: sigmap()
- Sigma minus: sigmam()
- Higher spin operators: jmat (j, s) where, j is the total spin and s can be 'x', 'y', 'z', '+', or '-'.

A.2. Functions on states and operators

States and operators can be further manipulated by calling inbuilt functions. In the list of functions below, a state or operator is represented as 'Q' and its inbuilt function is called via 'Q.function()'

- Conjugate: Q.conj()
- Adjoint: Q.dag()
- Eigenenergies: Q.eigenenergies()
- Eigenstates: Q.eigenstates(), this returns both eigenvalues and eigenvectors.
- Exponential: Q.expm(), matrix exponential of an operator.
- **Groundstate**: Q.groundstate()
- Norm: Q.norm(), returns L2 norm for states and trace norm for operators.
- Partial Trace: Q.ptrace(sel), returns partial trace with components selected using 'sel' parameter (see QuTip documentation for more details).
- Basis Transformation: Q.transform(ket_list), performs basis transformation to new basis given by 'ket_list', a list of states.
- Normalize a vector: Q.unit().

A.3. Evolution methods

QuDPy uses QuTip mesolve for the quantum evolution of a both closed and open systems. This function deploys the Schrödinger equation for closed and Lindblad equation for open quantum systems. See QuTip documentation for a detailed list of input parameters. Examples 1 and 2 also highlight specific use cases.

Appendix B. QuDPy functions and methods

The default System class variables are as follows

- $\hbar = 0.658211951$ in eV fs.
- ω , system frequency with a default value of E/\hbar with E=2 eV.
- H, Hamiltonian with default value of $\hbar\omega a^{\dagger}a$
- *a*, the system lowering operator for light-matter interaction. By default, it is the lowering operator of a 3-level harmonic oscillator.
- μ , the system dipole operator. Default value is $\mu = a^{\dagger} + a$
- c_ops, a list of collapse operators for Lindblad simulation. By default, it is empty.

Furthermore, the System class can be initialized with the following values.

- n, total energy levels.
- H, Hamiltonian
- rho, initial density matrix
- a, system lowering operator encoding emission of a photon.
- u, system dipole operator defined as $\mu(a^{\dagger}+a)$. $\mu=1$ typically.
- c_ops, list of collapse operators encoding system-bath coupling.
- e_ops (optional), list of operators for which expectation values are demanded in each simulation. Typically an empty list.
- tlist (optional), list of time steps for simulation. Typically not required during system initialization.
- diagonalize, True/False can perform Hamiltonian diagonalization and basis transformation of all operators if required.

B.1. Functions

The following functions are contained in the System class subroutine (see Fig. 4 for hierarchy details.

- diagram_donkey, for simulating a single trial of system
- coherence2d, for generating two-time coherence response.
- spectra, for converting the temporal response to spectra.
- linear spectra, for calculating and generating a linear
- pop_study, for computing a series of 2D-coherence

Similarly the $plot_functions$ subroutine contains the following functions,

- multiplot, for plotting multiple response (temporal or frequency) simultaneously.
- plot, for single spectrum or temporal response
- pop_plot, for plotting a response on multiple population times.

B.1.1. diagram_donkey

Computes and plots a single-density matrix evolution for a list of double-sided diagrams. Mainly useful for inspection/instructional purposes.

Inputs:

- interaction_times (required), a list of arrival times for pulses, and the last entry is the time interval for detecting a local oscillator.
- diagrams(required), a list of double-sided diagrams in UFSS diagramGenerator format.
- r (optional), temporal resolution (time steps per fs)

Outputs:

None, plots the diagram.

Notes:

The first pulse arrives at t=0.

B.1.2. coherence2d

Computes the 2D coherence plot for a single diagram with only two scanable delays. It can be parallelized if resources are available.

Inputs:

- time_delays (required), list of time delays. Provide a time delay for each interaction, even if zero. The default is None. These should be guided by experimental and theoretical considerations for each user.
- diagram (required), a double-sided diagram in UFSS diagramGenerator format. The default is None. Utilize desired phase-matching/phase-cycling conditions for diagram generation.
- scan_id (required), a list of indices for the time delays in interaction_times that must be scanned. Default is None
- r (optional), time resolution of simulation in steps per fs. The default value is 10. Should be guided by the energy eigenvalues of desired Hamiltonian.
- parallel (optional), parallelization control, True or False.
 Default is False

Outputs:

- A 2D list of density matrices for each pair of scanned times.
- A numpy array of first scan time
- A numpy array of second scan time
- ullet A 2D list of $\langle \mu \rangle$

Notes:

B.1.3. spectra

Converts the list of dipoles into spectra through Fourier transform.

Inputs:

- dipoles (required), a list of dipoles. Default is None
- resolution (optional), time resolution. The default is 10 steps per fs.

Outputs:

- List of spectra
- Minimum and maximum limits of each frequency axis
- · grid of first frequency
- · grid of second frequency

Notes:

B.1.4. linear_spec

For computing simple linear spectra from the system after any number of interactions in the start.

Inputs:

- scan_time (required), time interval to be simulated in fs.
- diagram (optional), double-sided diagram for calculating the system response. All interactions contained in the diagram are applied at t=0. If diagram=None, then by default, a 'Bu' interaction is applied at t=0.
- resolution (optional), time resolution of simulation in steps per fs.

Outputs:

- dipole expectation value
- time
- spectrum
- frequency

Notes:

For increasing the frequency resolution, increase the scan_time. To decrease the range of frequencies, decrease the time resolution

The function also plots the spectrum.

B.1.5. pop_study

For calculating the nonlinear response of a double-sided diagram for a set of population times.

Inputs:

- pop_time_list (required), a list of population times. Default None
- pop_index (required), an index of the population generating interaction. Default 1.
- time_delays (required), a list of time delays between interactions. Default None
- diagram (required), a double-sided diagram to be simulated.
 Default None
- scan_id (required), list of indices of time delays to be scanned for 2D coherence plot. Default None.
- r (optional), time resolution of simulation in steps per fs. The default is 10.
- parallel (optional), a True/False control of parallelized computation. Default is False

Outputs:

- list of 2D coherence response for each population time
- First scan time list
- Second scan time list
- List of spectra for each population time
- Extent of x and y-axis in spectra
- First frequency grid for spectra
- Second frequency grid for spectra.

Notes:

B.1.6. multiplot

Plot multiple data sets for spectral and evolution data.

Inputs:

- data (required), a list of spectra, dipole expectation values, or any other variable of interest. Default None
- scan_range (required), the min and max of both axis in the format [xmin, xmax, ymin, ymax]. Default None
- labels (required), a list of label for each axis. Default None
- title_list (required), a List of titles for each plot. Default None
- scale (optional), scaling of the data points, two choices are 'linear' and 'log'. Default 'linear'.
- color map(optional), choice of colormap. Default 'viridis'.
- interpolation (optional), interpolation for points in the plot, Default 'spline36'. Can be changed to None

Outputs:

Does not return any output, only generates the plots. ${\bf Notes:}$

B.1.7. plot

Plots a single data set.

Inputs:

- data (required), a spectrum or dipole expectation value list or any other variable of interest. Default None
- scan_range (required), the min and max of both axis in the format [xmin, xmax, ymin, ymax]. Default None
- label (required), a list of labels for each axis. Default None
- title list (required), a title for the plot. Default None
- scale (optional), scaling of the data points, two choices are 'linear' and 'log'. Default 'linear'.
- color map(optional), choice of colormap. Default 'viridis'.
- interpolation (optional), interpolation for points in the plot. Default 'spline36'. Can be changed to None

Outputs

Does not return any output, only generates the plot. **Notes:**

B.1.8. pop plot

Same as multiplot as of now. Will be updated in the future.

B.1.9. silva_plot

Plot multiple data sets for spectral and evolution data.

Inputs:

- spectra_list (required), a list of spectra, dipole expectation values, or any other variable of interest. Default None
- scan_range (required), the min and max of both axis in the format [xmin, xmax, ymin, ymax]. Default None
- labels (required), a list of label for each axis. Default None
- title_list (required), a List of titles for each plot. Default None
- scale (optional), scaling of the data points, two choices are 'linear' and 'log'. Default 'linear'.
- color map(optional), choice of colormap. Default 'PuOr'.
- interpolation (optional), interpolation for points in plot. Default 'spline36'. Can be changed to None.
- center_scale (optional), control for centering each data set in the list around zero by simple scale shift. The default value is True.
- plot_sum (optional), control for generating and plotting the total spectrum from the input list by summing individual data sets. Default True.
- plot_quadrant (optional), select a particular quadrant for the plot. Possible values are '1', '2', '3' and '4'. The default is 'All'
- invert_y (optional), control for inverting the y-axis by changing negative values to positive. Default is False
- diagonals (optional), list of True/False values for including (or excluding) the diagonal and cross diagonal reference lines. The default is [True, True]

Outputs:

Does not return any output, only generates the plots. **Notes:**

Appendix C. Functions and methods for defining model system with QuTip

C.1. Operators

The full details are available on the QuTip documentation. Briefly, the following operators can be defined to simulate a model Hamiltonian:

- destroy(N), Lowering operator for an N-level system
- imat(s,) defines a spin operator for a spin s system.

C.2. Functions

In addition to operators, the following operations and corresponding functions are available

- expectation value
- partace
- tensor

C.3. Methods quantum dynamics

The quantum evolution can be simulated by

- Schrodinger equation for closed systems
- Lindblad master equation for open quantum systems
- Redfield equation

References

- [1] F.D. Fuller, J.P. Ogilvie, Annu. Rev. Phys. Chem. 66 (1) (2015) 667–690, https://doi.org/10.1146/annurev-physchem-040513-103623, pMID: 25664841.
- [2] A.R. Srimath Kandada, H. Li, E.R. Bittner, C. Silva-Acuña, J. Phys. Chem. C 126 (12) (2022) 5378–5387, https://doi.org/10.1021/acs.jpcc.2c00658.
- [3] J.P. Ogilvie, K.J. Kubarych, in: Advances in Atomic Molecular and Optical Physics, in: Advances in Atomic, Molecular, and Optical Physics, vol. 57, Academic Press, 2009, pp. 249–321.
- [4] S. Mukamel, Annu. Rev. Phys. Chem. 51 (1) (2000) 691–729, https://doi.org/10. 1146/annurev.physchem.51.1.691, pMID: 11031297.
- [5] D.M. Jonas, Annu. Rev. Phys. Chem. 54 (1) (2003) 425–463, https://doi.org/10. 1146/annurev.physchem.54.011002.103907, pMID: 12626736.
- [6] M. Maiuri, M. Garavelli, G. Cerullo, J. Am. Chem. Soc. 142 (1) (2020) 3–15, https://doi.org/10.1021/jacs.9b10533, pMID: 31800225.
- [7] S. Mukamel, Principles of Nonlinear Optics and Spectroscopy, Oxford University Press, 1995.
- [8] P. Hamm, M. Zanni, Concepts and Methods of 2D Infrared Spectroscopy, Cambridge University Press, 2011.
- [9] J. Johansson, P. Nation, F. Nori, Comput. Phys. Commun. 184 (4) (2013) 1234–1240, https://doi.org/10.1016/j.cpc.2012.11.019.
- [10] P.A. Rose, J.J. Krich, J. Chem. Phys. 154 (3) (2021) 034109, https://doi.org/10. 1063/5.0024105.
 [11] P.A. Rose, J.J. Krich, J. Chem. Phys. 154 (3) (2021) 034108, https://doi.org/10.
- 1063/5.0024104.
 [12] T. Brixner, J. Stenger, H.M. Vaswani, M. Cho, R.E. Blankenship, G.R. Fleming,
- Nature 434 (2005) 625–628.

 [13] M. Cho, H.M. Vaswani, T. Brixner, J. Stenger, G.R. Fleming, J. Phys. Chem. B
- (2005) 10542–10556.
- [14] L. Yang, I.V. Schweigert, S.T. Cundiff, S. Mukamel, Phys. Rev. B 75 (2007) 125302.
- [15] Wei Zhuang, Darius Abramavicius, Tomoyuki Hayashi, Shaul Mukamel, J. Phys. Chem. B (2006) 3362–3374, https://doi.org/10.1021/jp055813u.
- [16] P.F. Tekavec, G.A. Lott, A.H. Marcus, J. Chem. Phys. 127 (21) (2007) 214307, https://doi.org/10.1063/1.2800560.
 [17] K.J. Karki, J.R. Widom, J. Seibt, I. Moody, M.C. Lonergan, T. Pullerits, A.H. Marcus,
- Nat. Commun. 5 (1) (2014) 5869, https://doi.org/10.1038/ncomms6869. [18] A.A. Bakulin, C. Silva, E. Vella, J. Phys. Chem. Lett. 7 (2) (2016) 250–258, https://
- [18] A.A. Bakulin, C. Silva, E. Vella, J. Phys. Chem. Lett. 7 (2) (2016) 250–258, https://doi.org/10.1021/acs.jpclett.5b01955.
- [19] E. Vella, H. Li, P. Grégoire, S.M. Tuladhar, M.S. Vezie, S. Few, C.M. Bazán, J. Nelson, C. Silva-Acuña, E.R. Bittner, Sci. Rep. 6 (1) (2016) 29437, https://doi.org/10.1038/srep29437.
- [20] H. Li, A. Gauthier-Houle, P. Grégoire, E. Vella, C. Silva-Acuña, E.R. Bittner, Chem. Phys. 481 (2016) 281–286, https://doi.org/10.1016/j.chemphys.2016.07.004.
- [21] Qutip Documentation, https://qutip.org/docs/latest/apidoc/functions.html#.
- [22] A. Redfield, in: J.S. Waugh (Ed.), Advances in Magnetic Resonance, in: Advances in Magnetic and Optical Resonance, vol. 1, Academic Press, 1965, pp. 1–32.
- [23] G. Lindblad, Commun. Math. Phys. 48 (2) (1976) 119–130, https://doi.org/10. 1007/BF01608499.
- [24] Pascal Gregoire, Étude de semi-conducteurs par spectroscopie d'excitation cohérente multidimensionnelle, PhD Thesis, Université de Montréal, 2017, https://doi.org/1866/20602.
- [25] Z. Vardeny, J. Tauc, Opt. Commun. 39 (6) (1981) 396–400, https://doi.org/10. 1016/0030-4018(81)90231-5.
- [26] R.H. Dicke, Phys. Rev. 93 (1954) 99-110, https://doi.org/10.1103/PhysRev.93.99.

- [27] F. Dimer, B. Estienne, A.S. Parkins, H.J. Carmichael, Phys. Rev. A 75 (2007) 013804, https://doi.org/10.1103/PhysRevA.75.013804.
 [28] D. Nagy, G. Kónya, G. Szirmai, P. Domokos, Phys. Rev. Lett. 104 (2010) 130401,
- https://doi.org/10.1103/PhysRevLett.104.130401.
- [29] K. Baumann, C. Guerlin, F. Brennecke, T. Esslinger, Nature 464 (7293) (2010) 1301–1306, https://doi.org/10.1038/nature09009.
 [30] M.M. Roses, E.G. Dalla Torre, PLoS ONE 15 (9) (2020) 1–8, https://doi.org/10.
- 1371/journal.pone.0235197.